Reaction fronts in a porous medium following injection along a temperature gradient

By T. E. JUPP AND A. W. WOODS

BP Institute for Multiphase Flow, University of Cambridge,
Madingley Road, Cambridge, CB3 0EZ, UK

(Received ?? and in revised form ??)

We consider the displacement of a 'formation fluid' by an 'injection fluid' along a temperature gradient in a reactive porous rock. We assume that the formation fluid is in chemical equilibrium initially and we allow the injection fluid to differ from the formation fluid both in temperature and in chemical composition. Two types of reaction front can form as the injection fluid propagates into the rock - (i) 'depletion fronts' caused by any undersaturation of the injection fluid and (ii) 'thermal reaction fronts' caused by any difference in temperature between the injection fluid and the trailing edge of the formation fluid. As flow proceeds the temperature gradient in the formation fluid is advected at the thermal propagation speed, but the fluid itself moves more quickly at the interstitial fluid speed. This difference in speed causes formation fluid to be carried out of chemical equilibrium and a 'gradient reaction' results. The subsequent dissolution or precipitation alters the amount of reactant present on the rock and this alters the propagation speed of any subsequent depletion front. We derive the six dimensionless parameters controlling the evolution of the system and calculate approximate solution profiles for the limit of fast kinetics and negligible diffusion. These solutions give insight into the physical processes governing the solution and are compared with numerical solutions of the full equations. The behaviour of the system is strongly influenced by three dimensionless parameters in particular. The parameters J_C and J_T quantify the chemical and thermal difference between the fluids at the point of injection and they control the relative positions of the depletion and thermal fronts at short times. On the other hand, the parameter α quantifies the background thermal gradient and controls the relative positions of the fronts at long times. In the cases where the depletion front moves from one side of the thermal front to the other, we derive approximate expressions for the time at which this 'crossover' occurs.

1. Introduction

In naturally occurring rocks, the geothermal temperature gradient may give rise to vertical temperature changes as large as $10°\text{C.km}^{-1}$. Since the equilibrium concentration of mineral species in solution varies with temperature, it follows that the pore-fluid can be stratified both in temperature and in chemical composition. This chemical stratification can lead to significant redistribution of minerals when the interstitial fluid is displaced by fluid flow. In particular, displacement of the fluid across the original isotherms results in under-saturation or super-saturation of the fluid, and associated precipitation or dissolution of mineral species [Phillips, 1991].

As an example, vertical displacement of fluid in geothermal systems may be driven by

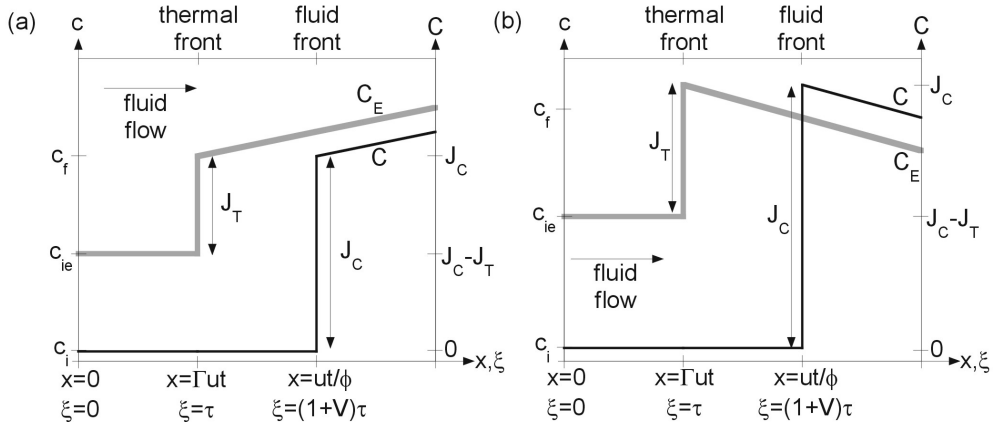

FIGURE 1. Sketches showing how the 'thermal' and chemical profiles would be advected downstream in the absence of diffusion and chemical reactions. The equilibrium concentration profile C_E (which is a proxy for temperature and shown in grey) is advected at speed Γu while the chemical profile C (shown in black) is advected at speed u/ϕ. (The corresponding dimensionless speeds, defined in §2, are 1 and $(1+V)$ respectively). After a time t the different speeds of advection have separated the two profiles. Chemical reactions would tend to drive dissolution or precipitation reactions where $C < C_E$ or $C > C_E$. Diffusion would tend to smooth out the sharp fronts shown here. (a) A 'positive' gradient in equilibrium concentration, in which C_E increases downstream; (b) As (a) but in the case of a 'negative' gradient (C_E decreases downstream).

buoyant convection associated with anomalous heat sources. More generally, displacement flows can develop in geological settings if a permeable rock is invaded by fluid from a source at higher pressure. Such flows may result from tectonic fracturing - which might connect one permeable layer to a deeper layer at higher pressure - or sea-level changes causing saline water to displace fresh water in coastal permeable rocks. In an industrial context, displacement flows often arise in hydrocarbon and geothermal reservoirs when water is injected into a reservoir in order to displace the formation fluid towards production wells.

A simple model for 'gradient reactions' - in which fluid is displaced along a temperature gradient - can be constructed as follows. In a rock with porosity ϕ and uniform temperature gradient G, a uniform flow with transport speed u along the gradient advects the isotherms at speed Γu where Γ is the ratio of specific heat of the fluid to that of the bulk [Jupp & Woods, 2003]. Assuming for simplicity that the equilibrium concentration of the fluid is a linear function of temperature ($c_e = a + bT$) it follows that the equilibrium concentration of the fluid at any fixed point in the rock evolves with time at a rate $bG\Gamma u$. Meanwhile the fluid moves through the pore spaces at the interstitial speed u/ϕ. The difference between the rate of advective transport of concentration along the temperature gradient, bGu/ϕ, and the local rate of change in concentration associated with the advection of the temperature field, $bG\Gamma u$, leads to reaction at a rate proportional to $bGu(1/\phi - \Gamma)$. This reaction may be one of precipitation or dissolution, depending on the sign of bG (Figure 1). We explore this model for gradient reactions in more detail in §3.

In addition to gradient reactions, any chemical or thermal differences between the injection and formation fluids can lead to the formation of travelling 'fronts'. We define the 'fluid front' to be the boundary between the injection and formation fluids. This is manifest as a jump in the chemical composition and moves at the interstitial fluid speed u/ϕ. In contrast, the thermal difference between the injection and formation fluids

defines a 'thermal front' which moves at the lesser speed Γu. The physical reason for this is that thermal signals travel through both the pore space and the rock, whereas chemical signals travel through the pore space alone. It follows that individual parcels of fluid travel faster than the thermal front and are able to cross it. These fluid parcels may experience a change in equilibrium concentration when crossing the thermal front leading to precipitation or dissolution reactions. The 'thermal front' can therefore induce a 'thermal reaction front' across which the concentration of the fluid changes. If the rock becomes depleted in reactant, however, reactions cease and the thermal reaction front can become decoupled from the thermal front to be advected downstream at the interstitial fluid velocity. If the injection fluid is undersaturated at the point of injection it will dissolve solid reactant there until the rock is fully depleted and a 'depletion front' forms. Upstream of a depletion front, the solid concentration is zero and no further reactions are possible.

The aim of this work is to explore how depletion and thermal reaction fronts are influenced by gradient reactions. The distinction between depletion fronts and thermal reaction fronts in porous rocks is discussed in detail by Jupp & Woods (2003). Our aim here is to complement that work by considering the influence of a gradient reaction associated with the flow.

The remainder of this paper is organised as follows. In §2, we develop a formal mathematical model for the system and derive the dimensionless parameters which govern its evolution. We also review the chemical balance relations which govern the speed at which reaction fronts move. In §3 we derive an analytical solution for the gradient reaction in the displaced formation fluid. In §4 we consider the interaction of a gradient reaction on the propagation of reaction fronts. In particular, we derive approximate solution profiles valid in the limit of 'fast kinetics' in which the advective supply of chemical reactant is rate limiting. These approximate solution profiles are compared with numerical solutions of the full governing equations. Finally, we give an estimate of the timescales over which different physical processes occur.

2. The governing equations

A full derivation of the governing equations used here is given by Jupp & Woods (2003). The equations in this present paper differ in the presence of a background temperature gradient in the initial conditions and in the chosen nondimensionalisation.

The evolution of temperature is controlled by an advection-diffusion equation of the form

$$\frac{\partial T}{\partial t} + \Gamma u \frac{\partial T}{\partial x} = D_T \frac{\partial^2 T}{\partial x^2}, \tag{2.1}$$

where D_T is the thermal diffusivity of the fluid-filled porous medium and Γ is the ratio of the volumetric heat capacity of the fluid to that of the the fluid-filled medium. For simplicity, we assume that the equilibrium concentration of the dissolved mineral species is a linear function of temperature, so that $c_e = a + bT$ where a and b are constants. The case $b > 0$ corresponds to a 'prograde' mineral whose solubility increases as temperature increases, while the case $b < 0$ corresponds to a 'retrograde' mineral whose solubility decreases as temperature increases. The assumption that $dc_e \propto \pm dT$ allows us to treat equilibrium concentration as a proxy for temperature. Consequently, all thermal effects are described in terms of the attendant change in equilibrium concentration. The first governing equation comes from rewriting the thermal balance of equation 2.1 in terms of

the equilibrium concentration:

$$\frac{\partial c_e}{\partial t} + \Gamma u \frac{\partial c_e}{\partial x} = D_T \frac{\partial^2 c_e}{\partial x^2}, \tag{2.2}$$

and we refer to the front which develops in the equilibrium concentration at $x = \Gamma u t$ as the 'thermal front'. Equation 2.2 is subject to the boundary condition

$$c_e(0,t) = c_{ie}, \quad t > 0 \tag{2.3}$$

and the initial condition

$$c_e(x,0) = c_f + bGx \tag{2.4}$$

where G is the initial thermal gradient.

The second governing equation controls the evolution of the fluid concentration c and is an advection-diffusion-reaction equation of the form

$$\frac{\partial c}{\partial t} + \left(\frac{u}{\phi}\right)\frac{\partial c}{\partial x} = D_C \frac{\partial^2 c}{\partial x^2} + k\left(\frac{s}{s_f}\right)(c_e - c), \tag{2.5}$$

where k is the reaction rate. Equation 2.5 is subject to the boundary condition

$$c(0,t) = c_i, \quad t > 0 \tag{2.6}$$

and the initial condition

$$c(x,0) = c_e(x,0) = c_f + bGx. \tag{2.7}$$

The third and final governing equation controls the evolution of the solid concentration s:

$$\frac{\partial s}{\partial t} = -k\frac{\phi}{\nu(1-\phi)}\left(\frac{s}{s_f}\right)(c_e - c). \tag{2.8}$$

where ν is a stoichiometric factor expressing the idea that ν moles of solid reactant may be required to react fully with each mole of fluid reactant. We suppose for simplicity that solid reactant is uniformly distributed through the rock initially so that equation 2.8 has the initial condition:

$$s(x,0) = s_f. \tag{2.9}$$

2.1. *Dimensionless form of the governing equations*

It is useful at this point to recast the governing equations 2.2, 2.5 and 2.8 in dimensionless form. The thermal front migrates with speed Γu, and so we introduce the dimensionless coordinates

$$\xi = \frac{k}{\Gamma u}x, \quad \tau = kt, \tag{2.10}$$

We also define the dimensionless concentrations

$$C(\xi,\tau) = \frac{\phi(c - c_i)}{(1-\phi)\nu s_f}, \quad C_E(\xi,\tau) = \frac{\phi(c_e - c_i)}{(1-\phi)\nu s_f}, \quad S(\xi,\tau) = \frac{s}{s_f}. \tag{2.11}$$

It follows from equations 2.2, 2.5 and 2.8 that the evolution of the system is governed by the dimensionless system of equations

$$\begin{aligned} \frac{\partial C_E}{\partial \tau} + \frac{\partial C_E}{\partial \xi} &= P\frac{\partial^2 C_E}{\partial \xi^2} \\ \frac{\partial C}{\partial \tau} + (1+V)\frac{\partial C}{\partial \xi} &= \epsilon P\frac{\partial^2 C}{\partial \xi^2} + S(C_E - C) \\ \frac{\partial S}{\partial \tau} &= -S(C_E - C) \end{aligned} \tag{2.12}$$

with initial conditions

$$C_E(\xi,0) = C(\xi,0) = J_C + \frac{\alpha}{V}\xi \quad \text{for} \quad \xi \geqslant 0 \tag{2.13}$$

$$S(\xi,0) = 1 \quad \text{for} \quad \xi \geqslant 0, \tag{2.14}$$

and boundary conditions

$$C_E(0,\tau) = J_C - J_T \quad \text{and} \quad C(0,\tau) = 0 \quad \text{for} \quad \tau > 0. \tag{2.15}$$

The six dimensionless parameters controlling the evolution of the system are therefore

$$\begin{aligned} V &= \frac{1-\phi\Gamma}{\phi\Gamma}, \qquad P = \frac{kD_T}{\Gamma^2 u^2}, \quad J_T = \frac{\phi(c_f - c_{ie})}{(1-\phi)\nu s_f}, \\ J_C &= \frac{\phi(c_f - c_i)}{(1-\phi)\nu s_f}, \quad \epsilon = \frac{D_C}{D_T}, \quad \alpha = \frac{bGu\,(1-\phi\Gamma)}{(1-\phi)\nu s_f k}. \end{aligned} \tag{2.16}$$

The parameter V is a measure of the relative speeds at which thermal and chemical signals are advected, since $V = (u/\phi - \Gamma u)/\Gamma u$. The parameter P can be interpreted as a dimensionless reaction rate. The governing equations show that chemical reaction occurs over a timescale $1/k$, while the thermal front becomes established on a timescale $D_T/\Gamma^2 u^2$. This is the value of time t at which the thermal front has been advected a distance Γut comparable to the distance $\sqrt{D_T t}$ that it has spread under dispersion and diffusion. Thus, P is the ratio of the timescale of formation of the thermal front $(D_T/\Gamma^2 u^2)$ to the timescale over which reactions occur $(1/k)$. The parameter J_T is a measure of the difference in temperature between the injection and formation fluids, expressed in terms of the attendant difference in equilibrium concentration. We shall show in §5.2 that J_T controls the initial speed of the thermal reaction front. The parameter J_C is a measure of the difference in concentration between the injection and formation fluids. We shall show in §5.1 that J_C controls the initial speed of the depletion front. Throughout this paper, we restrict attention to cases where the incoming fluid is either saturated $J_C = J_T$ or undersaturated $J_C > J_T$. We do not consider the case of oversaturated injection fluid ($J_C < J_T$) in which precipitation at the point of injection would tend to clog the pores of the rock. The parameter ϵ is the ratio of the chemical and thermal diffusivities. The parameter α is a dimensionless measure of the background thermal gradient and can be interpreted as the ratio of two rates. The quantity $bG\,(u/\phi - \Gamma u)$ is the rate of change of the equilibrium concentration c_e experienced by formation fluid as it travels at speed u/ϕ along the temperature gradient G which is advected at speed Γu. On the other hand, the quantity $(1-\phi)\nu s_f k/\phi$ is a measure of the rate at which the injection fluid concentration c can change under the influence of chemical reactions alone. The parameter α is the ratio of these two rates and so a small value of α indicates that the reaction rate is large compared to the rate of advective disequilibrium. We note for completeness that the special case $\alpha = 0$ is considered by Jupp & Woods (2003) in terms of the alternative dimensionless parameters $\lambda = J_C - J_T$ and $\beta = J_C/(J_C - J_T)$.

2.2. *Chemical balance at reaction fronts*

We now consider chemical balance at thermal reaction fronts and depletion fronts. In either case, the chemical balance at the front can be expressed in terms of the dimensionless variables defined in the previous section (Figure 2). For a front at $\xi = \xi_f$ moving at speed $V_f = d\xi_f/d\tau$, fluid particles move at a dimensionless speed $1 + V - V_f$ relative to the front and so there is a net molar flux $(1+V-V_f)(\Delta C)_f$ of dissolved reactant past the front. Similarly, there is a net molar flux $V_f(\Delta S)_f$ of solid reactant past the front. Chemical balance implies that these fluxes must be equal and so we deduce that the

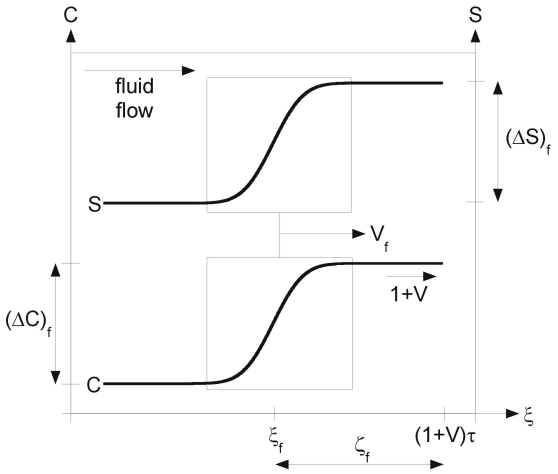

FIGURE 2. Chemical balance at a front (which may be a depletion front or a thermal reaction front). In the $\xi - \tau$ reference frame the front lies at ξ_f and moves at dimensionless speed V_f, while particles of fluid move at dimensionless speed $(1+V)$. The dimensionless distance between the front at ξ_f and the fluid front at $(1+V)\tau$ is denoted by ζ_f.

jump in solid concentration across the front $(\Delta S)_f$ and the jump in fluid concentration across the front $(\Delta C)_f$ must be linked by the equation:

$$V_f(\Delta S)_f = (1 + V - V_f)(\Delta C)_f \tag{2.17}$$

and so the speed of the front V_f is given by

$$\frac{d\xi_f}{d\tau} = V_f = \frac{1+V}{1 + \frac{(\Delta S)_f}{(\Delta C)_f}} \tag{2.18}$$

Later in this paper we shall make use of the variable $\zeta_f = (1+V)\tau - \xi_f$ representing the dimensionless distance between a front at $\xi = \xi_f$ and the fluid front at $\xi = (1+V)\tau$. It follows that

$$\frac{d\zeta_f}{d\tau} = 1 + V - V_f = \frac{1+V}{1 + \frac{(\Delta C)_f}{(\Delta S)_f}} \tag{2.19}$$

3. The gradient reaction solution in the formation fluid

The fluid front at $\xi = (1+V)\tau$ separates the formation fluid from the injection fluid. Diffusion tends to smooth the jump in concentration between the two fluids but has a negligible effect sufficiently far away from the front. Thus, an approximate solution within the displaced formation fluid (neglecting diffusive effects) is:

$$\begin{array}{rcl} C_E & = & J_C + \frac{\alpha}{V}(\xi - \tau) \\ C & = & J_C + \frac{\alpha}{V}(\xi - \tau) - (f(\tau) + \alpha\tau - 1) \\ S & = & f(\tau) \end{array} \tag{3.1}$$

where the governing equations 2.12 imply that the function $f(\tau)$ satisfies

$$\frac{\mathrm{d}f}{\mathrm{d}\tau} + \alpha\tau f + f(f-1) = 0, \quad f(0) = 1. \tag{3.2}$$

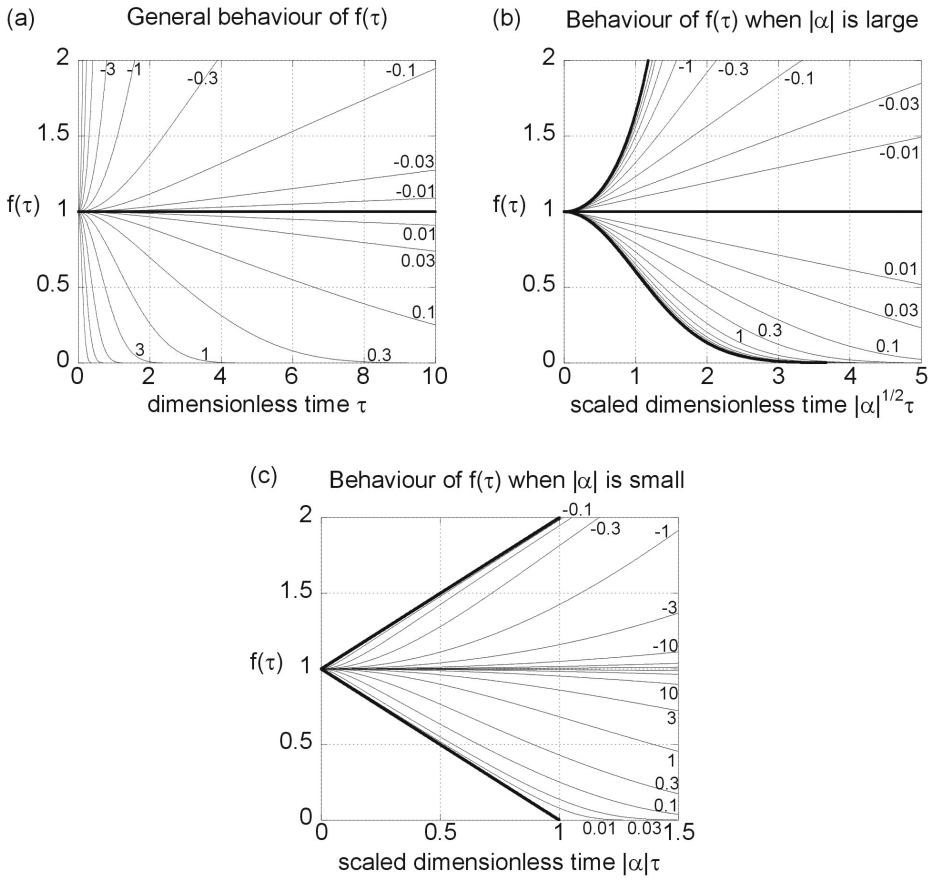

FIGURE 3. The behaviour of the function $f(\tau)$ (thin lines), representing the downstream value of the dimensionless solid concentration S. In each plot, $f(\tau)$ is shown for a range of values of α drawn from the set $\{\pm 0.01, \pm 0.03, \pm 0.1, \pm 0.3, \ldots, \pm 100\}$ with values of α shown in small type. (a) Plot of f against dimensionless time τ; (b) Plot of $f(\tau)$ against the rescaled time co-ordinate $\sqrt{|\alpha|}\tau$, showing that $f(\tau) \approx \exp(-\alpha\tau^2/2)$ (thick lines) when $|\alpha| \gg 1$; (c) Plot of $f(\tau)$ against the rescaled time co-ordinate $|\alpha|\tau$ showing that $f(\tau) \approx 1 - \alpha\tau$ (thick lines) when $\tau < 1/\alpha$ and $|\alpha| \ll 1$. When $\alpha < 0$ this linear behaviour is valid for all positive times, but when $\alpha > 0$, we have $f(\tau) \approx 0$ for $\tau > 1/\alpha$.

The solution of equation 3.2 can be calculated analytically and takes distinct forms depending on whether the gradient parameter α is zero, positive, or negative (Appendix A). Graphs of this solution are plotted in Figure 3, for a range of values of the gradient parameter α. Later in this paper, we shall make use of the function $f(\tau)$ and its definite integral $F(\tau) = \int_0^\tau f(t)\, dt$ (Appendix A). Although exact expressions for $f(\tau)$ and $F(\tau)$ can be derived (equations A 1 and A 2) they are complex and rather difficult to interpret. We shall therefore derive simple approximations for $f(\tau)$ and $F(\tau)$ in the limits $|\alpha| \ll 1$ and $|\alpha| \gg 1$.

3.1. *Approximate gradient reaction solutions when* $|\alpha| \ll 1$ *or* $|\alpha| \gg 1$

When the thermal gradient is very small or very large (in the sense that $|\alpha| \ll 1$ or $|\alpha| \gg 1$) the exact solution of equation A 1 can be replaced by simple approximations derived from series expansions (Appendix A).

If the dimensionless gradient is large ($|\alpha| \gg 1$) then gradient drives a reaction in which the reaction rate k is rate limiting. It can then be shown that

$$|\alpha| \gg 1 : \begin{cases} f(\tau) & \approx & \exp\left(-\frac{\alpha\tau^2}{2}\right) \\ F(\tau) & \approx & \begin{cases} \sqrt{\frac{\pi}{-2\alpha}}\operatorname{erfi}\left(\sqrt{\frac{-\alpha}{2}}\tau\right), & \alpha \ll -1 \\ \sqrt{\frac{\pi}{2\alpha}}\operatorname{erf}\left(\sqrt{\frac{\alpha}{2}}\tau\right), & \alpha \gg 1 \end{cases} \end{cases} \tag{3.3}$$

where $\operatorname{erf} x = \frac{2}{\sqrt{\pi}}\int_0^x \exp -y^2 \,\mathrm{d}y$ and $\operatorname{erfi} x = \frac{2}{\sqrt{\pi}}\int_0^x \exp y^2 \,\mathrm{d}y$. The solutions of equation 3.3 are illustrated in Figure 3b. When $\alpha \gg 1$, the gradient drives a dissolution reaction and so the downstream solid concentration is depleted to zero in a dimensionless time of order $1/\sqrt{\alpha}$. On the other hand, when $\alpha \ll -1$ the gradient drives a precipitation reaction and the downstream solid concentration increases for all time.

If the dimensionless gradient is small ($|\alpha| \ll 1$) then the gradient drives a reaction in which the advective supply of reactant is rate limiting. When this is a dissolution reaction ($0 < \alpha \ll 1$) we have:

$$0 < \alpha \ll 1 : \begin{cases} f(\tau) & \approx & \begin{cases} 1-\alpha\tau & \text{if} \quad \tau \leqslant 1/\alpha \\ 0 & \text{if} \quad \tau \geqslant 1/\alpha \end{cases} \\ F(\tau) & \approx & \begin{cases} \tau - \frac{1}{2}\alpha\tau^2 & \text{if} \quad \tau \leqslant 1/\alpha \\ 1/2\alpha & \text{if} \quad \tau \geqslant 1/\alpha \end{cases} \end{cases} \tag{3.4}$$

and so the downstream solid concentration is depleted linearly to zero in a dimensionless time of order $1/\alpha$ (Figure 3c). This corresponds to a dimensional time of order $\phi bG(u/\phi - \Gamma u)/(1-\phi)\nu s_f$ and so the time for downstream depletion is independent of the reaction rate k. This is precisely what we might expect since this is a regime in which the reaction rate is not rate-limiting.

When $|\alpha| \ll 1$ and the gradient drives a precipitation reaction, the dimensionless downstream solid concentration $f(\tau)$ no longer depletes to zero but grows indefinitely. In this case we obtain:

$$-1 \ll \alpha < 0 : \begin{cases} f(\tau) & \approx & 1-\alpha\tau \\ F(\tau) & \approx & \tau - \frac{1}{2}\alpha\tau^2 \end{cases} \tag{3.5}$$

For the remainder of this paper we restrict attention to the limit of fast kinetics ($|\alpha| \ll 1$) in which the approximations of equations 3.4 or 3.5 apply.

3.2. *The influence of the gradient reaction*

We showed in the previous section that the gradient reaction solution in the formation fluid is given by equation 3.1. We now consider how this gradient reaction affects the intruding injection fluid. Ultimately, we shall consider two regimes defined by the relative positions of the depletion front and the thermal front. Firstly, however, we illustrate the nature of the solution with some simple examples of numerical solutions of the equations. The solutions were calculated using the PDECOL solver package of Madsen & Sincovec (1979) as discussed by Hopkins (1992). This solver uses the method of lines, and a finite element collocation procedure is used for the spatial discretisation. The effects of

numerical dispersion were minimised in the simulations by the choice of a fine spatial mesh.

The simplest case of all is that in which there is no depletion front and no thermal front, so that $J_T = J_C = 0$ (Figures 4a,b). There is no depletion front because the incoming fluid is saturated and there is no thermal front because the injection fluid has the same temperature as the trailing edge of the formation fluid. At dimensionless time τ, the temperature of the injection fluid has been advected a dimensionless distance τ and so there is a change in the thermal gradient at $\xi = \tau$. Downstream of $\xi = \tau$ the different advective speeds of thermal and chemical signals mean that fluid is constantly carried out of chemical equilibrium and a gradient reaction results. When $\alpha > 0$ the gradient drives a depletion reaction (Figure 4a) and when $\alpha < 0$ it drives a precipitation reaction (Figure 4b). Upstream of $\xi = \tau$ the injection fluid is saturated so no reactions occur. This means that the passage of the gradient reaction is recorded on the rock as an altered value of the solid concentration S.

A depletion front can be added to the simple situations described above by allowing the incoming fluid to be undersaturated, so that $J_C > J_T$ (Figures 4c,d). The solution at the point of injection $\xi = 0$ then takes the simple form

$$C_E(0,\tau) = (J_C - J_T), \quad C(0,\tau) = 0, \quad S(0,\tau) = \exp\left(-(J_C - J_T)\tau\right) \tag{3.6}$$

It follows that the rock at the point of injection is depleted of solid reactant over a dimensionless timescale of order $1/(J_C - J_T)$ and so this can be interpreted as the dimensionless timescale over which the depletion front forms. Once the depletion front has formed it propagates into the medium at a speed governed by the amount of solid reactant it must dissolve to return to equilibrium according to the chemical balance of equation 2.18. It follows that the speed of the depletion front is influenced by the value of the solid concentration S that it encounters. The solid concentration records the legacy of the passage of the gradient reaction. When $\alpha > 0$ the gradient drives a dissolution reaction and so the solid concentration decreases downstream. The depletion front therefore accelerates over time as it must dissolve an ever decreasing amount of solid reactant. On the other hand, when $\alpha < 0$ the gradient reaction deposits solid reactant on the rock and so the solid concentration increases downstream. This means that the depletion front decelerates over time as it must dissolve an ever increasing amount of solid reactant.

A thermal front will develop if there is a difference in temperature between the injection fluid and the trailing edge of the formation fluid, so that $J_T \neq 0$ (Figures 5a,b). This thermal front tends to drive a dissolution reaction if $J_T > 0$ and a precipitation reaction if $J_T < 0$, but otherwise the situation is similar to those already discussed. Figure 5a illustrates a typical situation in which the depletion front lies downstream of the thermal front ('Regime 1'). The thermal front is unable to drive a reaction because it lies in a region which has already been depleted of solid reactant by the depletion front. On the other hand, Figure 5b illustrates a typical situation in which the thermal front lies downstream of the depletion front ('Regime 2'). In this case the thermal front is able to drive a reaction and so a thermal reaction front exists in addition to the depletion front.

4. Approximate solution profiles in the limit of fast reactions and negligible diffusion

In the previous section, we presented numerical solutions of the governing equations in order to illustrate how gradient reactions, depletion fronts and thermal fronts interact. We now derive approximate solution profiles in order to demonstrate the physical balances

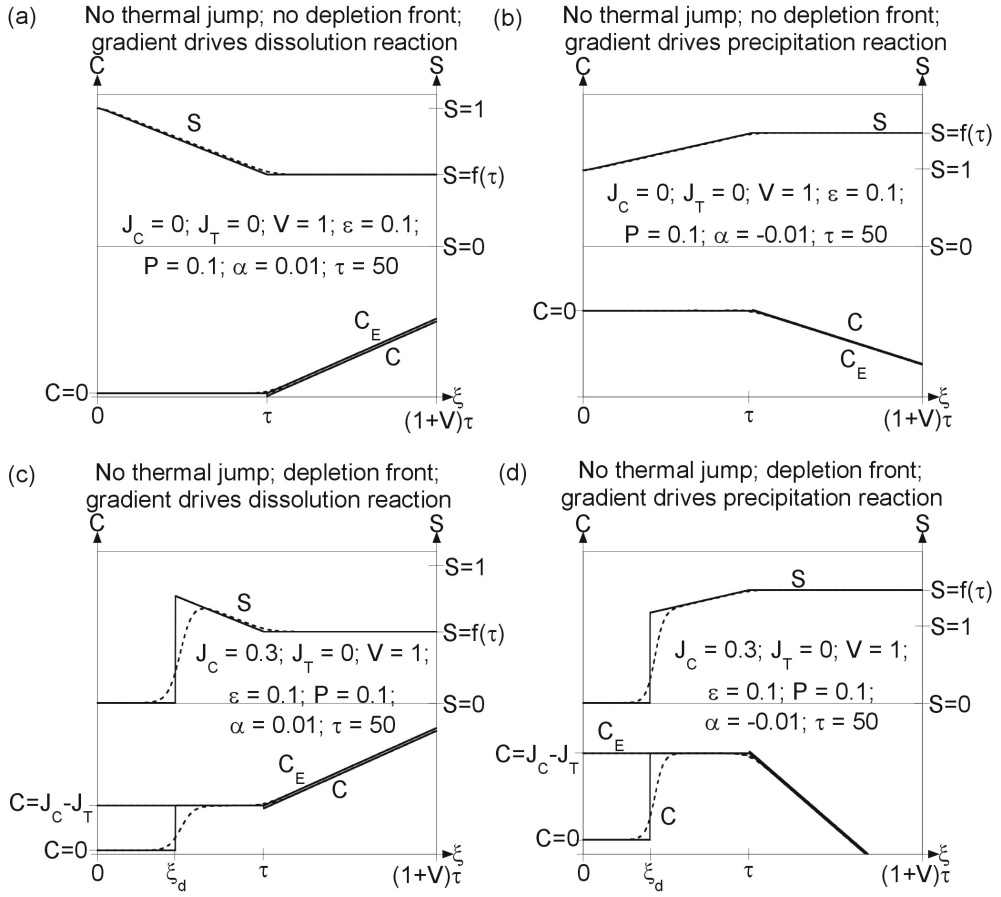

FIGURE 4. Solution profiles illustrating some simple cases. Numerical solutions of the full governing equations are shown (dotted lines) alongside approximate profiles (solid lines) calculated using the methods described in §4. Values of the dimensionless parameters are shown in each case, including the dimensionless time after injection τ. (*a*) The simplest case, in which there is no thermal jump ($J_T = 0$) and the injection fluid is saturated ($J_C = J_T$). Here $\alpha > 0$ and so the gradient drives a dissolution reaction; (*b*) As part (a) but with $\alpha < 0$ so that the gradient drives a precipitation reaction; (*c*) A more complicated case, in which a depletion front forms because the injection fluid is undersaturated ($J_C > J_T$); (*d*) As part (c) but with $\alpha < 0$.

	$\xi < \tau$	$\tau < \xi$
C_E	$J_C - J_T$	$J_C + \frac{\alpha}{V}(\xi - \tau)$

TABLE 1. Solution profile for the equilibrium concentration in the limit of negligible diffusion.

governing these interactions. For simplicity, we consider the limit in which diffusion is negligible and the reaction rate is not rate limiting for the gradient reaction ($|\alpha| \ll 1$). The approximate profile of the equilibrium concentration C_E is therefore given by the profile in Table 1.

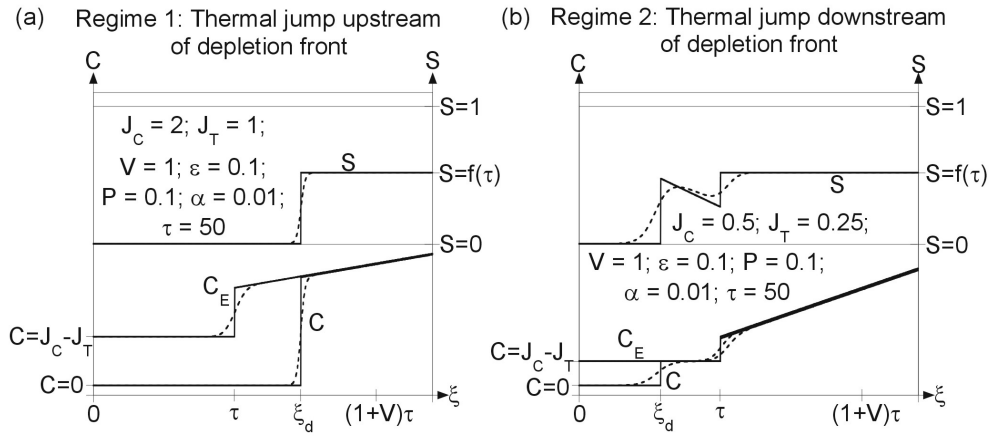

FIGURE 5. As figure 4, but showing solution profiles for the general case in which a gradient reaction, a depletion front and a thermal front are all present. (*a*) A typical solution in 'Regime 1' (depletion front downstream of thermal front); (*b*) A typical solution in 'Regime 2' (thermal front downstream of depletion front).

	$\xi < \xi_d$	$\xi_d < \xi$
C	0	$J_C + \frac{\alpha}{V}(\xi - \tau) - (f(\tau) + \alpha\tau - 1)$
S	0	$f(\tau)$

TABLE 2. Regime 1: approximate solution profiles for the fluid and solid concentrations when the depletion front lies downstream of the thermal front and the reaction rate is not rate-limiting ($|\alpha| \ll 1$).

4.1. *Regime 1: Depletion front lies downstream of thermal front*

Firstly, we consider 'Regime 1' in which the depletion front lies downstream of the thermal front (e.g. Figure 5a). The gradient reaction solution of equation 3.1 applies approximately as far upstream as the depletion front, since the reaction rate is large ($|\alpha| \ll 1$). It follows that the approximate solution profiles in Table 2 apply and so the jumps in fluid and solid concentration across the depletion front are:

$$\begin{array}{lcl} (\Delta C)_d & \approx & J_C + \frac{\alpha}{V}(\xi_d - \tau) - (f(\tau) + \alpha\tau - 1) \\ (\Delta S)_d & \approx & f(\tau) \end{array} \tag{4.1}$$

It then follows from equation 2.19 that $\zeta_d = (1+V)\tau - \xi_d$ evolves according to the equation:

$$\frac{d\zeta_d}{d\tau} \approx \frac{(1+V)f(\tau)}{1 + J_C - \alpha\zeta_d/V}. \tag{4.2}$$

In summary, when the system is in Regime 1, the approximate position of the depletion front can be calculated by integrating equation 4.2 and the approximate profiles are given by Tables 1 and 2, and are compared with full numerical solutions in figure 5a.

4.2. *Regime 2: Thermal front downstream of depletion front*

We now consider 'Regime 2' in which the thermal front lies downstream of the depletion front. In this case the gradient reaction solution of equation 3.1 applies (approximately)

	$\xi < \xi_d$	$\xi_d < \xi < \xi_t$	$\xi_t < \xi$
C	0	$J_C - J_T$	$J_C + \frac{\alpha}{V}(\xi - \tau) - (f(\tau) + \alpha\tau - 1)$
S	0	$\begin{cases} f(\xi) - V(\Delta C)_t, & \xi < \tau_{dc} \\ 0, & \xi \geqslant \tau_{dc} \end{cases}$	$f(\tau)$

TABLE 3. Regime 2: approximate solution profiles for the fluid and solid concentrations when the thermal front lies downstream of the depletion front and the reaction rate is not rate-limiting ($|\alpha| \ll 1$). The dimensionless decoupling time τ_{dc} is defined in the text.

as far upstream as the thermal reaction front (Figure 5b). The solid concentration downstream of the thermal reaction front is $f(\tau)$. At the thermal reaction front, the jumps in fluid and solid concentration are denoted by $(\Delta C)_t$ and $(\Delta S)_t$. The solid concentration S must always be non-negative and so $f(\tau)$ constitutes an upper bound for $(\Delta S)_t$. The speed of the thermal reaction front is governed by chemical balance (equation 2.18) and so the thermal reaction front can be 'coupled' to the thermal front only if $(\Delta S)_t = V(\Delta C)_t$. We deduce that

$$\begin{array}{rcl} (\Delta C)_t & \approx & J_T + \frac{\alpha}{V}(\xi_t - \tau) - (f(\tau) + \alpha\tau - 1) \\ (\Delta S)_t & \approx & \min\left(f(\tau), V(\Delta C)_t\right) \end{array} \tag{4.3}$$

In other words, if there is sufficient solid reactant downstream of the front then $(\Delta S)_t = V(\Delta C)_t$ and the thermal reaction front is coupled to the thermal front ($\xi_t = \tau$). On the other hand, if there is insufficient solid reactant downstream of the front then $(\Delta S)_t = f(\tau)$ and the thermal reaction front is decoupled from the thermal front ($\xi_t > \tau$).

We define the 'dimensionless decoupling time' τ_{dc} to be the least positive value of τ for which $f(\tau) = V(\Delta C)_t$ (if such a solution exists). This is the time at which the thermal reaction front becomes decoupled from the thermal front because of an insufficient supply of solid reactant.

We deduce that the approximate solution profiles given in Table 3 apply for Regime 2 and so the jumps in fluid and solid concentration at the depletion front are therefore:

$$\begin{array}{rcl} (\Delta C)_d & \approx & J_C - J_T \\ (\Delta S)_d & \approx & \begin{cases} f(\xi_d) - V(\Delta C)_t & \text{if} \quad \xi_d \leqslant \tau_{dc} \\ 0 & \text{if} \quad \xi_d > \tau_{dc} \end{cases} \end{array} \tag{4.4}$$

The speeds of the thermal reaction front can now be calculated using equations 4.3 and 4.4. It follows from equation 2.19 that $\zeta_t = (1+V)\tau - \xi_t$ evolves according to the equation

$$\frac{d\zeta_t}{d\tau} \approx \begin{cases} V & \text{if} \quad \tau \leqslant \tau_{dc} \\ \dfrac{(1+V)f(\tau)}{1 + J_T - \alpha\zeta_t/V} & \text{if} \quad \tau > \tau_{dc} \end{cases} \tag{4.5}$$

In the limit of fast reactions considered here, $|\alpha| \ll 1$, $(\Delta C)_t \approx J_T$ for $\tau < \tau_{dc}$. It then follows from equation 2.18 that the speed of the depletion front is given by:

$$\frac{d\xi_d}{d\tau} \approx \begin{cases} \dfrac{(J_C - J_T)(1+V)}{(J_C - (1+V)J_T) + f(\xi_d)} & \text{if} \quad \xi_d \leqslant \tau_{dc} \\ 1 + V & \text{if} \quad \xi_d > \tau_{dc} \end{cases} \tag{4.6}$$

In summary, when the system is in Regime 2, the approximate position of the thermal reaction front can be calculated by integrating equation 4.5 and the approximate position of the depletion front can be calculated by integrating equation 4.6. The approximate

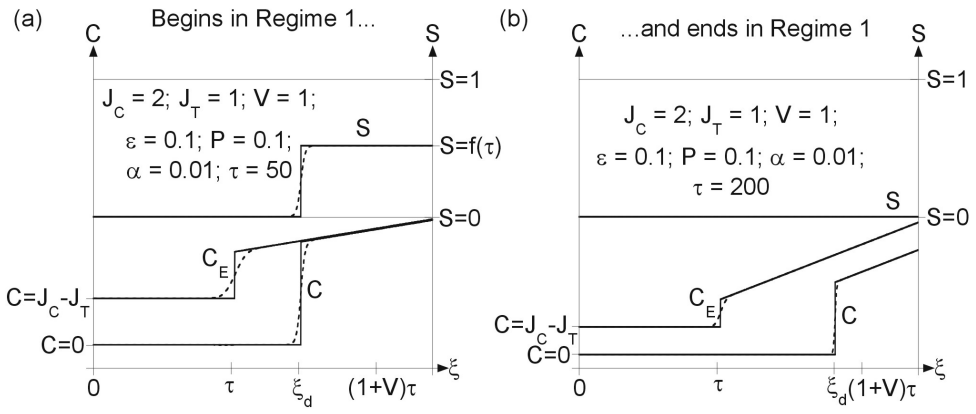

FIGURE 6. A typical solution when the system remains in Regime 1 for all time. Labelling as in Figure 4

.

solution profiles are given by Tables 1 and 3, and are compared with full numerical solutions in figure 5b.

5. Evolution of the system over time

In the previous section we defined the two solution regimes for the system according to the relative positions of the thermal and depletion fronts. The sign of the gradient parameter α determines whether the gradient drives a dissolution reaction or a precipitation reaction and hence whether the depletion front accelerates or decelerates over time. It is therefore possible for the system start in one regime but to move into a different regime for sufficiently long times.

5.1. *System begins in Regime 1*

If the system begins in Regime 1 then the approximate solution of Table 2 applies at short times (Figure 6a). Equation 4.1 shows that $(\Delta C)_d \to J_C$ and $(\Delta S)_d \to 1$ as $\tau \to 0$ and so we deduce from equation 2.18 that

$$\frac{d\xi_d}{d\tau} \to \frac{(1+V)}{1+1/J_C} \quad \text{as} \quad \tau \to 0 \quad \text{in Regime 1} \tag{5.1}$$

It follows that the system cannot be in Regime 1 at short times if $J_C < 1/V$. The position of the depletion front while the system remains in Regime 1 can be calculated approximately by integrating equation 4.2 with initial condition $\zeta_d(0) = 0$:

$$\zeta_d \approx \frac{V(1+J_C)}{\alpha}\left[1 - \sqrt{1 - \frac{2\alpha(1+V)F(\tau)}{V(1+J_C)^2}}\right] \tag{5.2}$$

We now consider whether the system can crossover into Regime 2.

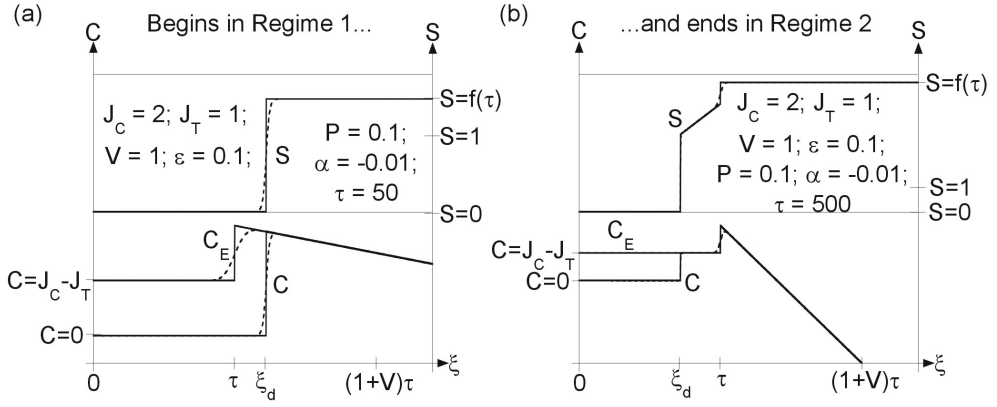

FIGURE 7. As Figure 6, but illustrating the case where the system begins in Regime 1 but moves into Regime 2 at long times.

If the gradient is small and positive ($0 < \alpha \ll 1$), it follows from equation 3.4 that:

$$\zeta_d \approx \begin{cases} \dfrac{V(1+J_C)}{\alpha}\left[1-\sqrt{1-\dfrac{\alpha(1+V)(2\tau-\alpha\tau^2)}{V(1+J_C)^2}}\right] & \text{for} \quad \tau < 1/\alpha \\ \dfrac{V(1+J_C)}{\alpha}\left[1-\sqrt{1-\dfrac{(1+V)}{V(1+J_C)^2}}\right] & \text{for} \quad \tau > 1/\alpha \end{cases} \tag{5.3}$$

This shows that, for dimensionless times greater than $1/\alpha$, the rock in the downstream region is fully depleted by the gradient reaction. The depletion front then moves at dimensionless speed $(1+V)$ and so ζ_d is constant.

On the other hand, if the gradient is small and negative ($-1 \ll \alpha < 0$) then the gradient drives a deposition reaction and the depletion front decelerates, eventually crossing to the upstream side of the thermal front at the 'crossover time' τ_c. This is the time for which $\zeta_d(\tau_c) = V\tau_c$ in equation 5.2. It follows (using equation 3.5) that:

$$\tau_c \approx \frac{2(1-VJ_C)}{\alpha} \tag{5.4}$$

when the system crosses from Regime 1 to Regime 2. A typical solution in which the system crosses from Regime 1 to Regime 2 is shown in Figure 7.

5.2. *System begins in Regime 2*

If the system begins in Regime 2, then the solution of Table 3 and equations 4.5 and 4.6 applies at short times. Equation 4.3 shows that $(\Delta C)_t \to J_T$ and $(\Delta S)_t \to \min(1, VJ_T)$ as $\tau \to 0$. It follows from equation 2.18 that

$$\frac{d\xi_t}{d\tau} \to \max\left(1, \frac{(1+V)}{1+1/J_T}\right) \quad \text{as} \quad \tau \to 0 \tag{5.5}$$

Since we consider only cases in which the injection fluid is undersaturated ($J_T \leqslant J_C$), it follows that the system begins in Regime 2 if $J_C < 1/V$.

If the gradient is small and negative ($-1 \ll \alpha < 0$) it drives a deposition reaction. The depletion front then decelerates over time and so the system remains in Regime 2 for all subsequent times. An example of this behaviour is shown in Figure 8.

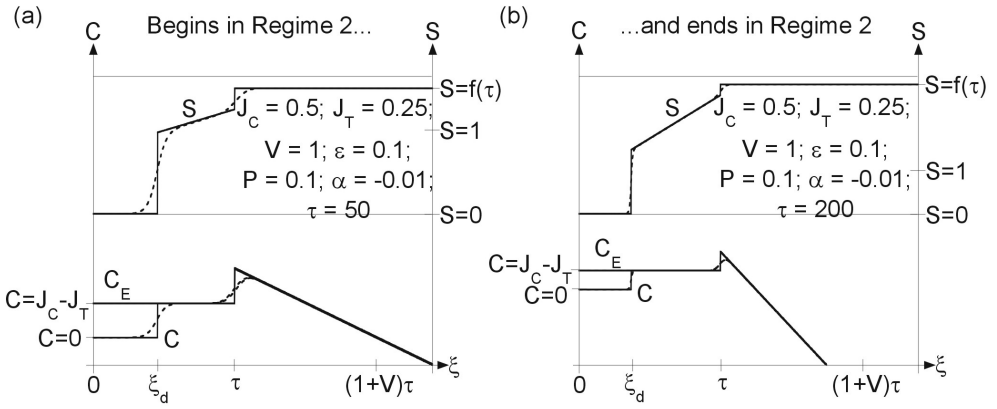

FIGURE 8. As Figure 6, but illustrating the case where there system remains in Regime 2 at all times.

On the other hand, if the gradient is small and positive ($0 < \alpha \ll 1$) it drives a dissolution reaction. The depletion front then accelerates over time and so the system eventually crosses into Regime 1 at the crossover time τ_c. The position of the depletion front, while the system remains in Regime 2, can be calculated approximately by integrating equation 4.6 with initial condition $\xi_d(0) = 0$. This gives

$$F(\xi_d) + (J_C - (1+V)J_T)\xi_d \approx (J_C - J_T)(1+V)\tau \tag{5.6}$$

and so the crossover time from Regime 2 to Regime 1 (for which $\xi_d(\tau_c) = \tau_c$) is

$$\tau_c \approx \frac{2(1 - VJ_C)}{\alpha}. \tag{5.7}$$

We note that this expression has the same form as the crossover time from Regime 1 to Regime 2 (equation 5.4). Equations 4.3 and 3.4 can be used to deduce that the decoupling time is

$$\tau_{dc} \approx \frac{1 - VJ_T}{\alpha}. \tag{5.8}$$

A typical solution in which the system moves from Regime 2 into Regime 1 is shown in Figure 9.

A summary of the timescales inherent in the problem is given in Table 4.

6. Discussion and Conclusions

We have considered the influence of a streamwise thermal gradient on a displacement flow in a reactive porous medium. We derived an analytical solution for the gradient reaction when the initial distribution of solid reactant is uniform and investigated the effect of this gradient reaction on the speeds and relative positions of thermal reaction fronts and depletion fronts.

Approximate solution profiles for the limit of no diffusion and fast kinetics were derived (Tables 1, 2, 3; Figures 6, 7, 8 and 9). These profiles give insight into the fundamental physics and are consistent with the results of numerical simulations . They also yield approximate expressions for the crossover time τ_c and the decoupling time τ_{dc} in the limit of fast kinetics ($|\alpha| \ll 1$) (Table 4).

When $0 < \alpha \ll 1$ the gradient drives a dissolution reaction. For sufficiently large times

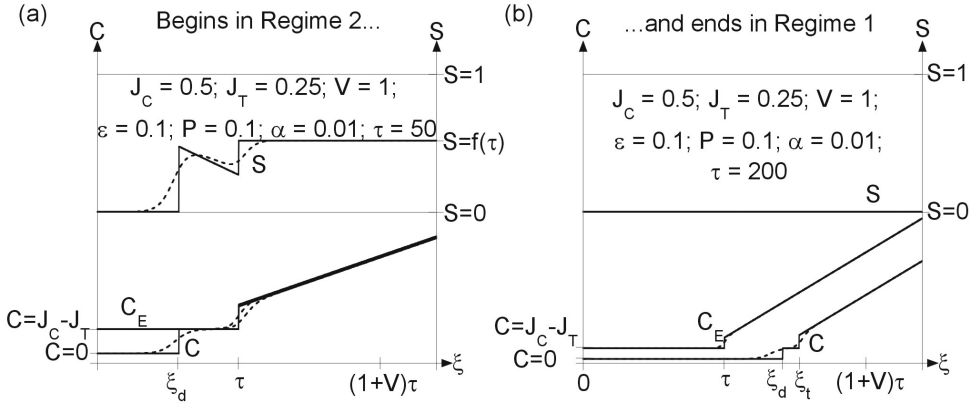

FIGURE 9. As Figure 6, but illustrating the case where the system begins in Regime 2 but moves into Regime 1 at long times.

Process	Dimensionless timescale
Chemical equilibration	1
Formation of thermal front	P
Formation of fluid front	$\epsilon P/(1+V)^2$
Formation of depletion front	$1/(J_C - J_T)$
Depletion by gradient reaction (if $0 < \alpha \ll 1$)	$1/\alpha$
Decoupling of thermal reaction front (if $0 < \alpha \ll 1$)	$\tau_{dc} \approx (1 - VJ_T)/\alpha$
Crossover of depletion front and thermal front (if $\lvert\alpha\rvert \ll 1$)	$\tau_c \approx 2(1 - VJ_C)/\alpha$

TABLE 4. The approximate dimensionless timescales associated with the evolution of the system, expressed in terms of the governing dimensionless parameters.

($\tau \gg 1/\alpha$), the downstream rock is totally depleted of reactant by the gradient reaction. It follows that no further reactions can occur and any frontal structure that has developed will simply advected downstream at dimensionless speed $(1 + V)$.

We derived the dimensionless parameters which govern the nature of the solution. In particular we showed how the solution depends on the three parameters α, J_C and J_T. The parameter α is a measure of the rate of advective supply to the gradient reaction in relation to the rate of chemical kinetics. The parameter J_C controls the position of the depletion front at short times $\tau \ll \tau_c$. If $J_C < 1/V$ the depletion front lies upstream of the thermal front at short times, while for $J_C > 1/V$ the depletion front lies downstream of the thermal front at short times. The parameter α controls the evolution of the speed of the depletion front, and hence whether it will 'crossover' from one side of the thermal front to the other. When $\alpha = 0$, the speed of the depletion front is constant [Jupp & Woods, 2003]. When $\alpha > 0$ the depletion front accelerates over time and when $\alpha < 0$ the depletion front decelerates over time. This behaviour is summarised in Figure 10.

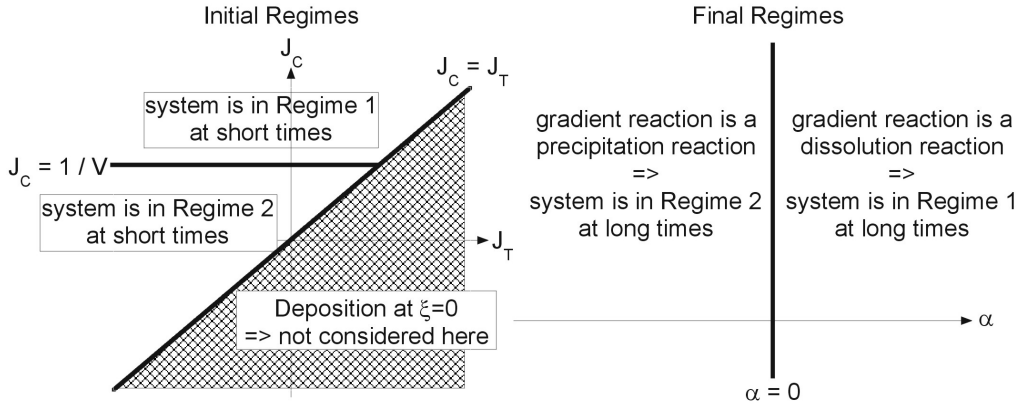

FIGURE 10. Diagrams illustrating how the parameters J_C and J_T control the regime of the system at short times, while the parameter α controls the regime of the system at long times.

In a real geological flow regime, we might expect fluid flow with transport velocity of order $10^{-8} - 10^{-7}$ m.s^{-1} and a background geothermal gradient G in the range $0.001 - 0.01$ K.m^{-1}. If the reaction rate k had a value in the range $10^{-4} - 10^{-6}$ s^{-1} (so that the reaction time k^{-1} ranged from a few hours to a few days), then we should expect that $\alpha \sim 10^{-4} - 10^{-2}$ and so the limit of fast kinetics investigated here would apply. For a rock with uniform mineral concentration at the start of the flow, the downstream concentration of mineral in the rock would decrease linearly with time after the start of the flow, as a result of the gradient reaction. This causes the thermal reaction front to decouple from the thermal front and migrate ahead of it. At long times, the thermal reaction front would lag a fixed distance behind the leading edge of the injected liquid. It follows that flow of this sort might lead to large zones of undersaturated water in the region between the thermal and thermal reaction fronts. The advance of the thermal reaction front leads to a more rapid depletion of the mineral content of the rock than would occur under the influence of the gradient reaction alone.

There may be a significant dynamic impact associated with the two different fronts. In particular, the change in temperature across the thermal front may lead to changes in fluid viscosity, porosity and permeability across the thermal reaction front. If the fronts lead to a decrease in mobility, then the flow across the front may become unstable, as with the acid etching instability [Hinch & Bhatt, 1990]. In a two or three dimensional flow, these fronts may also change the large scale structure of the flow [Menand et al., 2003]. Furthermore, in time dependent flows, such as those produced by sea-level change, reacting fluids may produce up to three zones of permeability and fluid within the rock, naturally leading to the formation of bands of mineralisation and stratification of the connate water.

This work has been supported by the BP Institute and the Newton Trust, Cambridge.

Appendix A. Exact solution for the gradient reaction

The substitution $u(\tau) = 1/f(\tau)$ can be used to derive an analytical solution of equation 3.2. This solution is:

$$f(\tau) = \begin{cases} \frac{\exp\left(-\frac{\alpha}{2}\left(\tau-\frac{1}{\alpha}\right)^2\right)}{\sqrt{\frac{\pi}{-2\alpha}}\left[\operatorname{erfi}\left(\sqrt{-\frac{\alpha}{2}}\left(\tau-\frac{1}{\alpha}\right)\right)-\operatorname{erfi}\left(\sqrt{\frac{-1}{2\alpha}}\right)\right]+\exp\left(\frac{-1}{2\alpha}\right)}, & \alpha<0 \\ 1, & \alpha=0 \\ \frac{\exp\left(-\frac{\alpha}{2}\left(\tau-\frac{1}{\alpha}\right)^2\right)}{\sqrt{\frac{\pi}{2\alpha}}\left[\operatorname{erf}\left(\sqrt{\frac{\alpha}{2}}\left(\tau-\frac{1}{\alpha}\right)\right)-\operatorname{erf}\left(-\sqrt{\frac{1}{2\alpha}}\right)\right]+\exp\left(\frac{-1}{2\alpha}\right)}, & \alpha>0 \end{cases} \tag{A 1}$$

where $\operatorname{erf} x = \frac{2}{\sqrt{\pi}}\int_0^x \exp -y^2 \, \mathrm{d}y$ and $\operatorname{erfi} x = \frac{2}{\sqrt{\pi}}\int_0^x \exp y^2 \, \mathrm{d}y$. By definition, $F(\tau) = \int_0^\tau f(t)\, dt$, and so equation A 1 can be integrated to give:

$$F(\tau) = \begin{cases} \log\left[\sqrt{\frac{\pi}{-2\alpha}}\left(\operatorname{erfi}\left(\sqrt{\frac{-\alpha}{2}}\left(\tau-\frac{1}{\alpha}\right)\right)-\operatorname{erfi}\left(\frac{1}{\sqrt{-2\alpha}}\right)\right)+\exp\left(\frac{-1}{2\alpha}\right)\right]+\frac{1}{2\alpha}, & \alpha<0 \\ \tau, & \alpha=0 \\ \log\left[\sqrt{\frac{\pi}{2\alpha}}\left(\operatorname{erf}\left(\sqrt{\frac{\alpha}{2}}\left(\tau-\frac{1}{\alpha}\right)\right)-\operatorname{erf}\left(\frac{-1}{\sqrt{2\alpha}}\right)\right)+\exp\left(\frac{-1}{2\alpha}\right)\right]+\frac{1}{2\alpha}, & \alpha>0 \end{cases} \tag{A 2}$$

The following series can be truncated to give asymptotic expressions in the limit $x \to 0$ [Abramovitz & Stegun, 1964].

$$\begin{gathered} \exp(x) = \textstyle\sum_{k=0}^{\infty} \frac{x^k}{k!}, \quad \operatorname{erf}(x) = \frac{2}{\sqrt{\pi}} \sum_{k=0}^{\infty} \frac{(-1)^k x^{2k+1}}{(2k+1)k!} \\ \operatorname{erfi}(x) = \frac{2}{\sqrt{\pi}} \sum_{k=0}^{\infty} \frac{x^{2k+1}}{(2k+1)k!} \end{gathered} \tag{A 3}$$

The following series can be truncated to give asymptotic expressions in the limit $x \to \infty$ [Abramovitz & Stegun, 1964].

$$\operatorname{erf}(x) = 1 - \frac{\exp\left(-x^2\right)}{x\sqrt{\pi}} \sum_{k=0}^{\infty} \frac{(-1)^k (2k)!}{k!\,(2x)^{2k}}, \quad \operatorname{erfi}(x) = \frac{\exp\left(x^2\right)}{x\sqrt{\pi}} \sum_{k=0}^{\infty} \frac{(2k)!}{k!\,(2x)^{2k}} \tag{A 4}$$

REFERENCES

Abramowitz, M. & I. A. Stegun (eds.) 1964 *Handbook of Mathematical Functions with Formulas, Graphs and Mathematical Tables, Vol. 55 of National Bureau of Standards Applied Mathematics Series.*, Washington, D.C.: U.S. Government Printing Office.

Hinch, E. J. & Bhatt, B. S. 1990 Stability of an acid front moving through porous rock. *J. Fluid Mech.* **212**, 279–288.

Hopkins, T. 1992 Remark on "Algorithm 540: PDECOL, General Collocation Software for Partial Differential Equations [D3]". *ACM Transactions on Mathematical Software* **18**, 343–344.

Jupp, T. E. & Woods, A. W. 2003 Thermally driven reaction fronts in porous media. *J. Fluid Mech.* **484**, 329–346.

Madsen, N.K. & Sincovec, R.F. 1979 Algorithm 540: PDECOL, General Collocation Software for Partial Differential Equations [D3]. *ACM Transactions on Mathematical Software* **5**, 326–351.

Menand, T., Raw, A. & A.W. Woods 2003 Thermally inertia and reversing buoyancy in flow in porous media. *Geophys. Res. Lett.* **30**(6), doi:10.1029/2002GL016294.

Phillips, O. M. 1991 *Flow and Reactions in Permeable Rocks*, pp. 359–384. Cambridge University Press.